Electron-F_2O collision study using the *R*-matrix method

Monika Gupta and K. L. Baluja
Department of Physics and Astrophysics, University of Delhi, Delhi 110007, India
(Received 22 August 2006; published 27 November 2006)

The present study deals with the calculation of differential, elastic integral, momentum transfer, and excitation cross sections for electron-F_2O collision in a 16-state *R*-matrix method. Configuration interation (CI) wave functions are used to represent the target states. The CI model gave an adequate description of the vertical excitation spectrum from the equilibrium geometry of the ground state X^1A_1 of the F_2O molecule that spans the energy range 4.21–10.21 eV. Our calculated dipole moment of 0.224 D is in good agreement with the experimental value 0.297 D. We also found two broad shape resonances in $^2A_1$ and $^2B_2$ scattering symmetries and both resonances support dissociative electron attachment. A born correction is applied for the elastic and dipole allowed transitions to account for higher partial waves ($l>4$) excluded in the *R*-matrix calculation. All cross sections are presented for incident electron energies up to 15 eV. Our results are compared with cross sections of Cl_2O calculated at the same level of complexity using the *R*-matrix method.

DOI: 10.1103/PhysRevA.74.052713 PACS number(s): 34.80.Bm, 34.80.Gs, 34.80.Ht

I. INTRODUCTION

The study of spectroscopy of Cl_xO_y compounds and the electron-impact study on these molecules has recently received much attention [1–3] due to the direct or indirect involvement in the chain reaction occurring in the high terrestrial atmosphere leading to the much concerned ozone depletion. However, the F_2O (difluorine monoxide), which has an isovalence electronic structure with Cl_2O and belongs to the same point group C_{2v} has been neglected both theoretically and experimentally. Its experimental absorption spectrum is still unknown and there are no electron scattering calculations available for the F_2O molecule. Its photoelectron spectrum in the outer-valence region was first recorded by Cornford *et al.* [4] and Brundle *et al.* [5]. Cornford *et al.* [4] studied the photoelectron spectroscopy of F_2O and determined the valence molecular orbitals.

Various experimental studies have determined the structural parameters of F_2O by using electron diffraction [6–9]. Hilton *et al.* [10] and Pierce *et al.* [11] determined the bond length FO and the apex angle by using microwave spectroscopy. The dipole moment of F_2O at its equilibrium geometry was determined [11] by a quantitative Stark effect measurement of $1_{01}\rightarrow 1_{10}$ and $2_{02}\rightarrow 2_{11}$ transitions which yield a value of 0.297 ± 0.005 D. However, there is a serious disagreement with the dipole moment measurement of Bransford *et al.* [12] who incorrectly assigned the rotational transitions. The molecular geometry, molecular *g* values, the magnetic susceptibilities, the molecular quadrupole moments, and the second moments of the electronic charge distribution for F_2O have been determined by the rotational Zeeman effect [13].

Self-consistent field (SCF) calculations for F_2O have been carried out by Rothenberg and Schaefer [14] in which the energetics and population analysis were performed. They also computed the dipole and quadrupole moment at the experimental equilibrium geometry of F_2O. Valenta *et al.* [15] carried out SCF and a large scale configuration interaction (CI) calculation using a double-zeta plus polarization (DZP) basis set augmented with Rydberg type functions to compute the vertical electronic excitation energies of only the lowest two singlet and two triplet excited states for each symmetry of a C_{2v} point group of F_2O. They assigned the valence and/or Rydberg character to the electronic states studied by them. Thiel *et al.* [16] carried out SCF and CI calculations with single and double excitation using DZP and TZP basis sets and computed the dipole moment of F_2O at its equilibrium geometry. Tomasello *et al.* [17] used a symmetry-adapted-cluster-configuration interaction (SAC-CI) method to calculate few singlet excited states of each symmetry lying below the first IP (13.75 eV). They compared the calculated SAC-CI spectrum of F_2O with Cl_2O and found that each state is blueshifted by 2–4 eV. They conclude that the valence-excited states exist lower in energy than the Rydberg states, which are found above 10 eV. The $\langle r^2\rangle$ values for valence states lie between 126–128, which approximately have the same value as the ground state. Tomasello *et al.* [17] also gave detailed characterizations of the valence and Rydberg excited states by calculating oscillator strengths, second moments, and the dipole moment. In a more recent work, Tomasello *et al.* [18] have given detailed theoretical ionization spectra of the F_2O molecule in the outer and intermediate valence region.

In the present work, the calculations are carried out by using UK polyatomic *R*-matrix codes [19,20]. This code has recently been used on H_2CO [21], O_3 [22], and SO_2 [23]. The calculation of rotationally elastic and inelastic DCS is carried out by using the program POLYDCS [24]. The *K*-matrix elements required by this program are calculated in a 16-state *R*-matrix approach where each state is represented by a CI configuration. This is a comprehensive treatment of electron impact on F_2O molecule using an *ab initio* method.

II. *R*-MATRIX THEORY

The central idea underlying the *R*-matrix method [25,26] is that the scattering problem is split into two separate spatial regions, an inner region and an outer region. The inner region is chosen in such a way that the charge density of the target is negligible at the boundary of the inner region and

outer region. It is defined in the present case by a sphere of radius 10 a_o centered at the F_2O center of mass. In the inner region, the scattering electron cannot be distinguished from the electrons of the target making the problem hard but solvable. When the scattering electron is at a large distance from the center of mass of the target, the probability of swapping its identity with any of the target electrons is negligible. This simplifies the problem in the outer region considerably. In the inner region, the wave function is written using the CI expression:

$$\Psi_k^{N+1} = A \sum \Phi_i^N(x_1, \ldots, x_N) \sum \xi_j(x_{N+1}) a_{ijk} + \sum \chi_m(x_1, \ldots, x_N, x_{N+1}) b_{mk}, \quad (1)$$

where A is an antisymmetrization operator, x_N is the spatial and spin coordinate of the Nth electron, ϕ_i^N represents the ith state of the N-electron target, ξ_j is a continuum orbital spin-coupled with the target states. The continuum functions are the only functions with finite amplitudes on the R-matrix boundary. The sum in the second term of Eq. (1) represents short-range polarization effects. To obtain reliable results, it is important to maintain a balance between the N-electron target representation, ϕ_i^N, and the $(N+1)$ electron scattering wave function. The choice of appropriate χ_m is crucial in this [27]. The coefficients a_{ijk} and b_{mk} are variational parameters which can be determined by solving an eigenvalue problem relevant to the inner region, where all the relevant integrals are evaluated for the spatial range 0–10 a_0 by employing the standard bound state quantum chemistry methods. In practice, all the integrals are evaluated in the entire configuration space; the tail contribution outside the R-matrix sphere is then subtracted.

In the first term of Eq. (1), the first summation is over the number of target electronic states included in the calculation and the second summation is over the number of continuum orbitals linked to each target state. The double summation in the first term of Eq. (1) generates "target+continuum" configurations. The summation in the second term of Eq. (1) runs over configurations χ_m, where all electrons are placed in target occupied and virtual molecular orbitals. These are described as the L^2 configurations and are important for relaxing the orthogonality between the target and continuum orbitals. Gaussian-type orbitals (GTOs) are used to represent the bound and the continuum electrons. The main advantage of GTOs is that the multicentered integrals can be evaluated in a closed form. We have used the GTO continuum basis functions of Faure *et al.* [28] in which these functions were fitted to Bessel functions for the case of a neutral molecule.

In the outer region, when the scattering electron is at a large distance from the center of mass of the target, the probability of swapping its identity with any of the target electron is negligible and so are the exchange and correlation effects. The interacting potentials are direct and are multipolar in character. We include only the dipolar and quadrupolar potentials of the long-range character. The outer region is essentially a potential-field region, and we can use a single center expansion of the scattering system analogous to Eq. (1) by dropping the antisymmetrization operator and also dropping the second summation involving correlation effects. This leads to a set of coupled differential equations, and the solution functions are propagated outward [29] until the effect of multipolar forces is negligible. These solutions are then matched with the appropriate standing wave boundary conditions yielding K matrix, eigenphase sums, and the cross sections.

III. RESULTS AND DISCUSSION

A. Target model of F_2O

The calculations on F_2O in the present work used the double-zeta plus-polarization (DZP) Gaussian basis set (11,5,1)/[4,3,1] for F and (9,5,1)/[4,2,1] for O [30]. We have not used a large basis set with diffuse functions as it extends outside the R-matrix box. F_2O belongs to the point group C_{2v}, which is of order four and its ground state, is represented by X^1A_1 symmetry. Here we have used the experimental geometry with R (F-O)=1.405 Å and θ (FOF) =103.1° [11]. F_2O is formed by bonding each of the two unpaired $2p$ orbitals of fluorine with the unpaired $2p$ orbitals of oxygen. The Hartree-Fock electronic configuration for the ground state is

$$1b_2^2 1a_1^2 2a_1^2 3a_1^2 2b_2^2 4a_1^2 1b_1^2 5a_1^2 3b_2^2 1a_2^2 4b_2^2 6a_1^2 2b_1^2.$$

The molecular orbitals are generated by performing a self-consistent field (SCF) calculation at the experimental equilibrium geometry of the ground state of the F_2O molecule. These SCF wave functions of the target are calculated from standard contracted basis set and the SCF energy is found to be −273.5288 a.u. In the present work, CI wave functions are used to represent all the target states. Here, we keep the core 6 electrons fully occupied in the 3 molecular orbitals, $1a_1$, $2a_1$, and $1b_2$ and the remaining 20 valence electrons are free to occupy $3a_1$, $4a_1$, $5a_1$, $6a_1$, $7a_1$, $1b_1$, $2b_1$, $2b_2$, $3b_2$, $4b_2$, $5b_2$, and $1a_2$ molecular orbitals. The vertical excitation energies for the 15 states so formed lie in the range 4.21–10.01 eV, which agree well with the theoretical values [15,17].

In Table I, we list the dominant configuration, the number of configuration state functions (CSFs), the transition moments, and the vertical excitation energies for the first nine states. The remaining seven excited states are not shown as these are included to check convergence of our results and also to avoid any unphysical pseudoresonances that may otherwise appear in the cross section. To provide additional information on the charge distribution in F_2O molecule, we have also calculated the dipole and quadrupole moments of F_2O at its equilibrium geometry. Our SCF model yields a dipole moment of 0.423 D for F_2O at its equilibrium geometry. This value is much higher than the experimental value, 0.297 D [11]. The corresponding value obtained by our CI model with a DZP basis set is 0.224 D, which is in good accord with the experimental value. The absolute values of quadrupole components Q_{20} and Q_{22} for the ground state in our CI model are 0.331 au and 0.155 au, respectively.

Our calculations included the 16 target states in the close-coupling expansion [see Eq. (1)]. Calculations were per-

TABLE I. Dominant configuration, transition moment of each transition from the ground state in (au), the number of configurations, N, and the vertical excitation energies in eV for the target states of F_2O.

State	Configuration	Transition moment (au)	N	Vertical excitation energies (eV)		
				This work	Valenta *et al.* 1980	Tomasello *et al.* 2002
X^1A_1	$6a_1^2 2b_1^2 4b_2^2 1a_2^2$	0.0885[a]	480			
$1\,^3B_1$	$(\cdots)\ 2b_1^{-1}7a_1$	0.0000	524	4.21	3.82	
$1\,^3A_2$	$(\cdots)\ 2b_1^{-1}5b_2$	0.0000	529	4.99	4.66	
$1\,^1B_1$	$(\cdots)\ 2b_1^{-1}7a_1$	0.1174	396	5.48	5.36	5.36
$1\,^1A_2$	$(\cdots)\ 2b_1^{-1}5b_2$	0.0000	396	6.04	5.91	6.05
$1\,^3A_1$	$(\cdots)\ 6a_1^{-1}7a_1$	0.0000	546	7.16	6.92	
$1\,^3B_2$	$(\cdots)\ 6a_1^{-1}5b_2$	0.0000	556	7.34	6.84	
$2\,^3B_2$	$(\cdots)\ 4b_2^{-1}7a_1$	0.0000	556	7.98	7.44	
$1\,^1B_2$	$(\cdots)\ 4b_2^{-1}7a_1$	0.0434	444	8.02	7.76	8.17

[a]Dipole moment.

formed for doublet A_1, A_2, B_1, and B_2 scattering symmetries. The continuum orbitals were represented by Gaussians centered at the molecule center of gravity to represent Bessel functions within the finite region of the R-matrix sphere [27]. These orbitals depend parametrically on the R-matrix spherical radius and the range of incident electron-impact energies, and are independent of the target molecule. Our calculations were performed for continuum orbitals up to g-partial wave. These continuum orbitals were orthogonalized to the target orbitals based on a mixture of Schmidt and Löwdin symmetric orthogonalization methods, and those continuum orbitals with an overlap of less than 2×10^{-7} were removed [19]. It is important to preserve the balance between the amount of correlation included in the target states and in the scattering calculation. This is achieved by allowing 21 electrons (20 valence electrons+1 scattering electron) to move freely among $3a_1$, $4a_1$, $5a_1$, $6a_1$, $7a_1$, $1b_1$, $2b_1$, $2b_2$, $3b_2$, $4b_2$, $5b_2$, and $1a_2$ molecular orbitals.

B. Differential cross sections

Chang and Temkin [31] have shown that the rotational excitation cross sections for electron impact on a neutral molecule can be accurately calculated from the scattering parameters of elastic scattering in the fixed nuclei approximation provided the nuclei are assumed to be of infinite masses. In particular, starting from an initial rotor state $J=0$, the sum of all transitions from $J=0$ level to a high enough J value for convergence is equivalent to the elastic cross section in the fixed nuclei approach. We have employed this methodology to extract rotationally elastic and inelastic cross sections from the K-matrix elements calculated in the 16-state R-matrix method. The evaluation of DCS is a stringent test for any scattering theory employed. The DCS for a general polyatomic molecule is given by the familiar expression

$$d\sigma/d\Omega = \sum A_L P_L(\cos\theta), \tag{2}$$

where P_L is a Legendre function. The A_L coefficients have already been discussed in detail [32]. For a polar molecule this expansion over L converges slowly. To circumvent this problem, we use the closure formula

$$d\sigma/d\Omega = d\sigma^B/d\Omega + \sum (A_L - A_L{}^B) P_L(\cos\theta). \tag{3}$$

The superscript B denotes that the relevant quantity is calculated in the Born approximation with an electron-point dipole interaction. The convergence of the series is now rapid since the contribution from the higher partial waves to the DCS is dominated by the electron-dipole interaction. The quantity $d\sigma^B/d\Omega$ for any initial rotor state $|J\tau\rangle$ is given by the sum over all final rotor states $|J'\tau'\rangle$.

$$d\sigma^B/d\Omega = \sum d\sigma^B/d\Omega(J\tau \to J'\tau'). \tag{4}$$

The expressions of state-to-state rotationally inelastic DCS, $d\sigma^B/d\Omega$ $(J\tau \to J'\tau')$, for a spherical top, a symmetric top, and an asymmetric top molecule are given by Sanna and Gianturco [24]. The rotational eigenfunctions and energy levels of F_2O, which is an asymmetric top molecule, are calculated by the program ASYMTOP [33] for all values of J up to 5. The eigenvalues are reported in Table II. We used the calculated rotational constants for F_2O at its equilibrium geometry, which are 1.960 78 cm^{-1}, 0.363 47 cm^{-1}, and 0.305 79 cm^{-1}. Since there is no vacancy in the ground state of F_2O molecule, the scattering electron can occupy one of the low-lying virtual orbitals $7a_1$ and $5b_2$, which have SCF orbital energies +3.61 eV and +4.78 eV, respectively at the equilibrium geometry of the F_2O molecule. We found R-matrix poles at −273.607 11 au, −273.551 42 au, −273.587 41 au, and −273.589 06 au, in the scattering symmetries $^2A_1$, $^2A_2$, $^2B_1$, and $^2B_2$, respectively. The values are higher than the energy −273.62 75 au of the ground state $X\,^1A_1$ of the F_2O molecule implying that these scattering symmetries are not bound at the equilibrium geometry of the molecule.

We have calculated DCS for elastic scattering of electrons from F_2O molecule at incident electron energies 1.4, 2.8, 6, 10, and 15 eV in the angular range from 0° to 180°. In this we included the first low-lying 16 states in the close coupling

TABLE II. Energies of rotational levels of electron-F_2O scattering system.

J	τ	Energy (meV)
0	0	0.0
1	−1	0.083
	0	0.281
	1	0.288
2	−2	0.248
	−1	0.440
	0	0.461
	1	1.055
	2	1.055
3	−3	0.497
	−2	0.678
	−1	0.720
	0	1.304
	1	1.304
	2	2.311
	3	2.311
4	−4	0.827
	−3	0.996
	−2	1.066
	−1	1.635
	0	1.638
	1	2.644
	2	2.644
	3	4.054
	4	4.054
5	−5	1.238
	−4	1.393
	−3	1.497
	−2	2.050
	−1	2.056
	0	3.059
	1	3.059
	2	4.469
	3	4.469
	4	6.283
	5	6.283

expansion. The K-matrix elements from a particular scattering R-matrix calculation form input to the computational code [24] which yields the DCS, elastic, and momentum transfer cross sections. In Fig. 1, we have displayed DCS at 1.4 eV for state-to-state rotational excitation cross section for initial state $J=0$ to final state $J'=0,1,2,3,4,5$. This energy corresponds to the resonance energy of the shape resonance of $^2A_1$ scattering symmetry (see Sec. III C). For angles less than 70°, the elastic component dominates over other inelastic components. We notice a strong forward peak for the dipole allowed $0\rightarrow1$ transition which is a characteristic of the dipole nature of the target molecule. For this dipole transition, there are two minima around 30° and 90° with a maximum in between at around 60°. The transition $0\rightarrow2$ is governed by the quadrupole moment of the molecule, and the cross section for this transition is almost flat with a value of about 2 Å^2/sr. The cross section for $0\rightarrow3$ transition rises monotonically from low scattering angles to higher scattering angles. The remaining components are quite small thereby showing that our DCS cross section shown by summing over all final J' values has converged with respect to the J' values included in the present calculation.

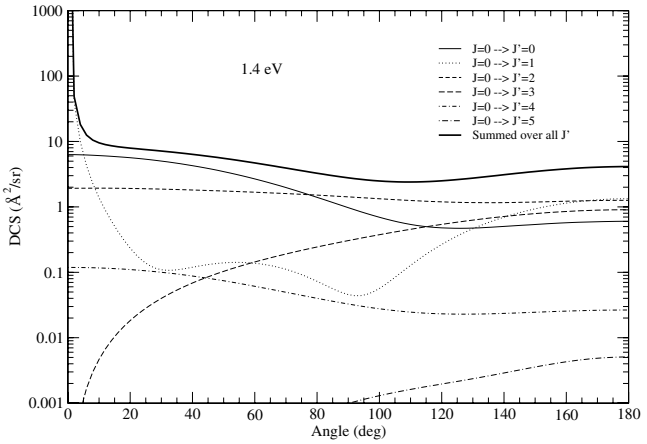

FIG. 1. DCS at 1.4 eV: Full curve, $J=0\rightarrow J'=0$ transition; dotted curve, $J=0\rightarrow J'=1$ transition; small dashed curve, $J=0\rightarrow J'=2$ transition; long dashed curve, $J=0\rightarrow J'=3$ transition; dot-small dashed curve, $J=0\rightarrow J'=4$ transition; dot-long dashed curve, $J=0\rightarrow J'=5$ transition; dark solid curve, summed over all J and J'.

A similar situation is maintained in Fig. 2, which is depicted at electron impact energy of 2.8 eV, chosen to coincide with the resonance position of the $^2B_2$ shape resonance (Sec. III C). In Fig. 3, we show the DCS at 6 eV, 10 eV, and 15 eV. At these energies, the cross section drops quickly in the angular range 0°–5° then decreases up to about 100° and finally rises marginally in the backward direction.

C. Elastic integral and momentum transfer cross sections

Figure 4 shows our static-exchange (SE), static-exchange plus polarization (SEP), and 16-state R-matrix CI elastic in-

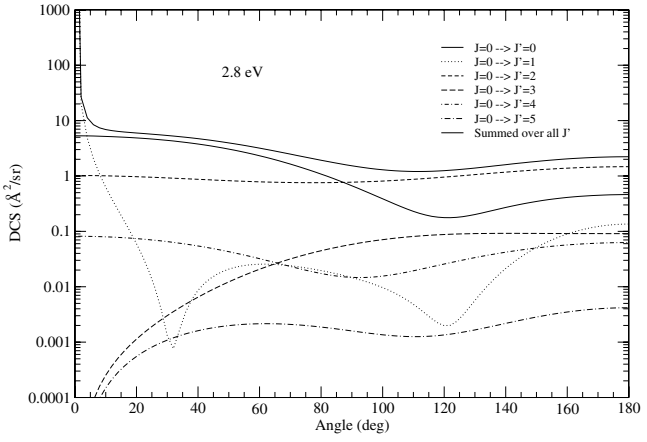

FIG. 2. DCS at 2.8 eV: Same as Fig. 1.

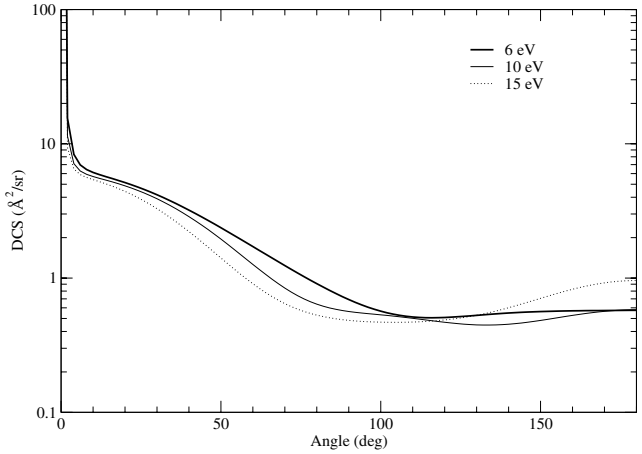

FIG. 3. DCS's at different energies: Dark solid curve, 6 eV; full curve, 10 eV; dotted curve, 15 eV.

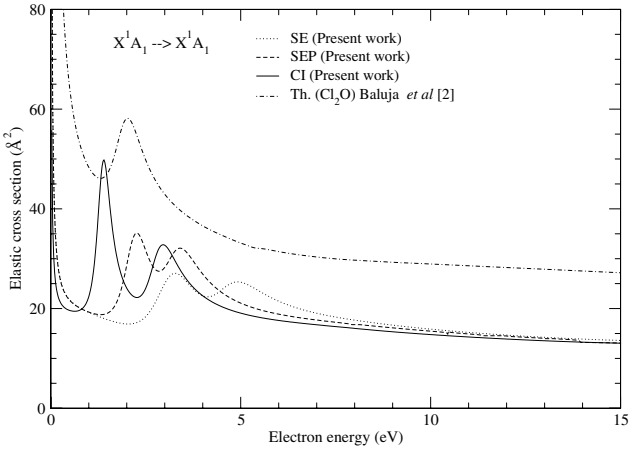

FIG. 4. Elastic cross sections for electron impact on F_2O: dotted curve, SE; dashed curve, SEP; full curve, CI (16-state *R*-matrix); theory (Cl_2O): dot-dashed curve, Baluja *et al.* Ref. [2].

tegral cross sections. The main feature in the elastic cross section is the presence of two shape resonances in $^2A_1$ and $^2B_2$ symmetry. In a shape resonance phenomenon, the incident electron with a nonzero angular momentum, is trapped by the centrifugal barrier to form a temporary negative molecular ion F_2O^- that decays via quantum mechanical tunneling. These resonances are not characterized only by mere structures in the cross sections but are connected with a sudden increase of about Π radian in the eigenphase sum in a multichannel calculation. By fitting the eigenphase sum to the Breit-Wigner profile [34] we can determine the resonance parameters for the resonances. In the SE calculation, we find shape resonances at 3.2 and 4.9 eV in $^2A_1$ and $^2B_2$ symmetry, respectively while in SEP calculation these resonances shift to lower energies at 2.2 and 3.3 eV, respectively. This shift is caused by the inclusion of correlation effects. The SEP results usually suffer from the balancing problem of correlations so we performed a full CI calculation including 16 state and the resonances then shifted to 1.4 and 2.8 eV.

We have shown in Table III the resonance parameters along with the configuration assignment for these shape resonances. The $^2A_1$ and $^2B_2$ scattering symmetries contribute significantly to the elastic cross section as compared to the contribution of other two scattering symmetries $^2B_1$ and $^2A_2$. Since no other experimental or theoretical work for the determination of scattering cross sections of F_2O is available to date, we have compared our elastic cross sections with the elastic cross sections of Cl_2O [2] since F and Cl are isovalent. Baluja *et al.* [2] have calculated the cross section for electron scattering from Cl_2O using the *R*-matrix method in which they included the first low-lying 16-states with

TABLE III. Resonance states of electron-F_2O system.

Resonance No.	Symmetry	Parameters E_r (eV)	Parameters Γ_r (eV)	Assignment	Type of Resonance
1	$^2A_1$	1.4	0.463	$(X^1A_1)\ 7a_1$	Shape
2	$^2B_2$	2.8	0.887	$(X^1A_1)\ 5b_2$	Shape

R-matrix radius fixed at 10 a_o. This calculation employed up to *f*-partial waves in the *R*-matrix treatment. For consistency with the present work, we have extended this calculation (Cl_2O) by including up to *g*-partial waves to represent the continuum orbitals. Since Cl is a much heavier atom, we notice the cross sections for Cl_2O are much larger than the cross section for F_2O. In contrast to only one shape resonance of symmetry $^2B_2$ in Cl_2O at 2.1 eV, we have two shape resonances of symmetries $^2B_2$ and $^2A_1$ in the F_2O case. The $^2A_1$ anionic state of Cl_2O^- is electronically bound and therefore no resonance shows up in $^2A_1$ symmetry. The SCF value of 10 a_1 virtual lowest unoccupied molecular orbital (LUMO) for Cl_2O is only 1.35 eV [2]. The $^2B_2$ symmetry resonance in F_2O occurs at a higher energy (~0.7 eV) than the corresponding case of Cl_2O. The higher nuclear charge of Cl is responsible for this behavior. Beyond the resonance region, both the curves for cross section of Cl_2O and F_2O are almost parallel to each other in the energy range 6–15 eV. The cross section for Cl_2O are larger by a factor of almost two which is nearly the same ratio between the number of electrons in Cl_2 and F_2. We also repeated the calculations for elastic scattering of electrons from Cl_2O and F_2O by increasing the *R*-matrix radius to 12 a_o. For Cl_2O, the increase in *R*-matrix radius had an insignificant effect on the cross sections including the resonance position and its peak value. However, for F_2O, the calculation at *R*-matrix radius equal to 12 a_o, had a small effect on elastic scattering cross sections between 10–15 eV range. The maximum difference was about 10% at 12 eV. There was no change in the resonance parameters.

The inclusion of correlation in the target states and the loss of flux in the additional scattering channels provided in a multistate calculation lowers the cross sections in a CI calculation. Due to the presence of a long-range dipole interaction, the elastic cross section is formally divergent in the fixed-nuclei approximation due to a singularity in the differential cross section in the forward direction. To obtain converged cross sections, the effect of rotation must be included along with a very large number of partial waves. The effect of partial waves higher than an $l=4$ partial wave were in-

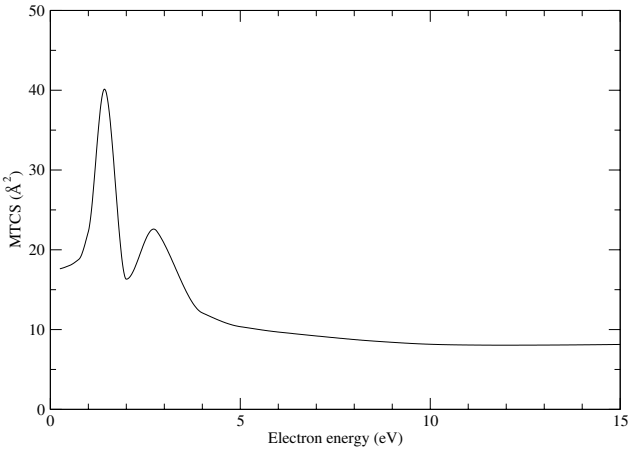

FIG. 5. Momentum transfer cross section for electron scattering by F_2O: full curve, present work (16-state R matrix).

cluded using a Born correction which requires expressions for the partial as well as full Born cross sections. These expressions have been taken from the work of Chu and Dalgarno [35]. For applying the Born correction we have used the experimental value 0.1169 au for the dipole moment of F_2O at its equilibrium geometry.

We have also calculated the momentum transfer cross section (MTCS), defined as follows:

$$\sigma_m = 2\pi \int d\sigma/d\Omega(1 - \cos\theta)d\theta. \tag{5}$$

The MTCS gives an indication of the backward scattering. The MTCS is an important parameter in solving the Boltzmann equation for the calculation of electron distribution function and the drift velocity of a swarm of electrons moving through a particular medium. The effect of shape resonances at 1.4 and 2.8 eV is reflected quite clearly in MTCS at these energies in Fig. 5. Beyond 5 eV, the MTCS remain nearly constant.

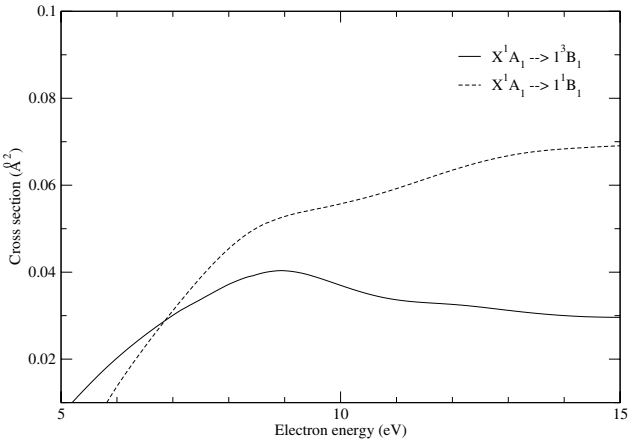

FIG. 6. Electron impact R-matrix excitation cross sections: Full curve, $X^1A_1 \rightarrow 1^3B_1$ symmetry; dashed curve, $X^1A_1 \rightarrow 1^1B_1$ symmetry.

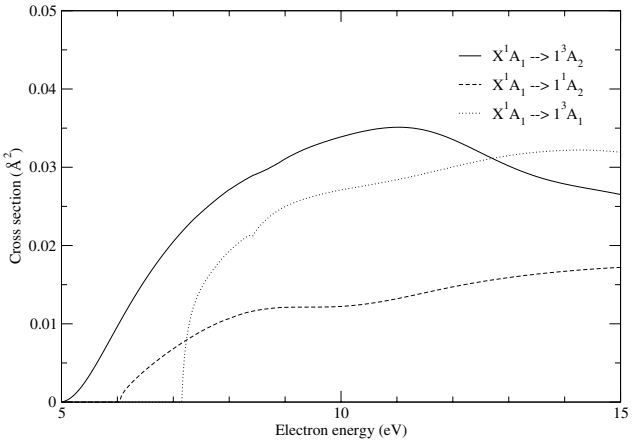

FIG. 7. Electron impact R-matrix excitation cross sections: Full curve, $X^1A_1 \rightarrow 1^3A_2$ symmetry; dashed curve, $X^1A_1 \rightarrow 1^1A_2$ symmetry, dotted curve, $X^1A_1 \rightarrow 1^3A_1$ symmetry.

D. Inelastic cross sections

Figures 6–8 present electron-impact excitation cross sections from the ground state to the first eight excited states, but the results shown are for our best 16-state calculation. According to the optical dipole selection rules, the transitions to the triplet states are spin forbidden, and the transitions to the states of A_2 symmetry are symmetry forbidden. The transitions to excited states of $^1B_1$ and $^1B_2$ symmetry are dipole allowed out of which the transition to a $^1B_1$ excited state is stronger due to its higher transition moment of 0.1174 au. The cross sections for these dipole allowed transitions have been Born corrected.

In Fig. 6 we have presented the excitation cross sections from the ground state to the excited states: 1^3B_1 and 1^1B_1. The cross section for 1^3B_1 excited state rises monotonically up to 9 eV and then becomes nearly constant in the energy range 10–15 eV. Since the transition to a 1^1B_1 state is dipole allowed from the ground state, its cross section is higher than its corresponding triplet component in the energy region away from thresholds.

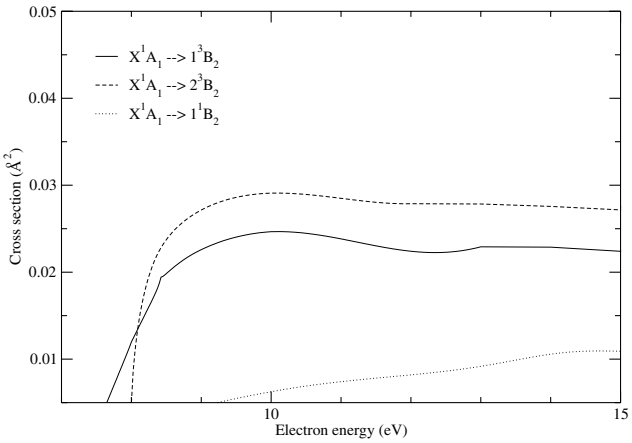

FIG. 8. Electron impact R-matrix excitation cross sections: full curve, $X^1A_1 \rightarrow 1^3B_2$ symmetry; dashed curve, $X^1A_1 \rightarrow 2^3B_2$ symmetry, dotted curve, $X^1A_1 \rightarrow 1^1B_2$ symmetry.

Figure 7 shows the cross sections for the transitions $X^1A_1 \rightarrow 1^3A_2$, 1^1A_2, and 1^3A_1. For 1^3A_2 cross section, the maximum contribution comes from $^2B_2$ scattering symmetry whereas for 1^1A_2, all the symmetries contribute significantly. For 1^3A_1 excited state, $^2A_1$ contributes nearly 70% to the cross section, the other contribution comes from $^2B_2$ scattering symmetry. All the cross sections shown in this figure are quite small (<0.04 Å^2) due to the spin-forbidden and symmetry-forbidden nature of the transitions.

The cross sections for B_2 symmetries are shown in Fig. 8. These cross sections are also very small due to the spin-forbidden nature of triplet excited states transition from the ground state. Even though the transition $X^1A_1 \rightarrow 1^1B_2$ is dipole allowed but its transition moment is negligible and due to its high threshold of 8.02 eV, the corresponding cross section are small.

IV. DISSOCIATIVE ELECTRON ATTACHMENT

The present study identifies the presence of shape resonances in symmetries $^2A_1$ and $^2B_2$. To explore the possible dissociative nature of resonant states, we have investigated its dependence by performing calculations in which one F-O bond and the FOF angle are kept fixed at their equilibrium values and the other F-O bond is stretched from its equilibrium value to 8.0 a_0. This stretching mode asymptotically correlates to the following two-body fragmentation channels:

$$F_2O^- \rightarrow FO + F^-,$$

$$F_2O^- \rightarrow FO^- + F.$$

The calculations are performed in a C_s point group, in which A' symmetry correlates with A_1 and B_2 symmetries of a C_{2v} point group and the other A'' symmetry of C_s correlates with the other two symmetries of a C_{2v} point group. Variation of resonant states is thus explored via A' symmetry only. In Fig. 9, we have shown the variation of resonance width of $^2A_1$ and $^2B_2$ shape resonances with a stretching bond. The resonance width for both the scattering symmetries tends to zero around 3.0 a_0, which implies that these resonances become bound and support dissociative electron attachment. The electron affinity (EA) of the dissociated products helps in assigning the preference of the scattering electron to attach to a particular fragment. Since the EA of FO (2.272 eV) is less than EA of F (3.401 eV) we expect the formation of F^- ions to be more likely.

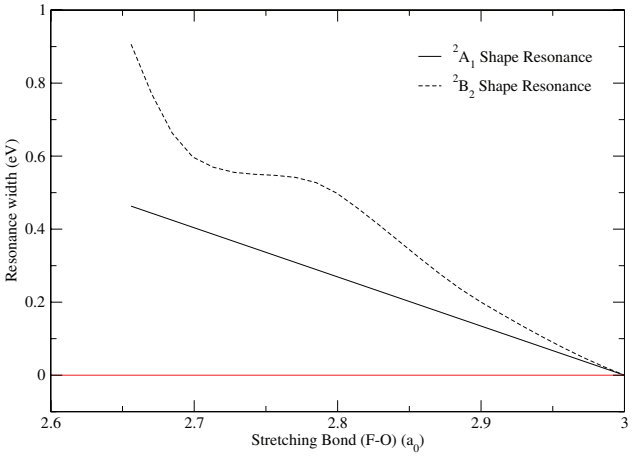

FIG. 9. (Color online) Variation of resonant width ($^2A_1$ and $^2B_2$) with F-O stretching: full curve, resonance width, $^2A_1$ shape resonance; dashed curve, resonance width, $^2B_2$ shape resonance.

V. CONCLUSIONS

This is a detailed *ab initio* study of electron impact on the F_2O molecule. The elastic differential, integral, momentum transfer, and excitation cross sections for electron impact on F_2O are calculated using the *R*-matrix method with good target representation. The value of dipole moment obtained is in good agreement with the experimental value. Our calculation detects shape resonances in $^2A_1$ and $^2B_2$ scattering symmetries at the equilibrium geometry of F_2O molecule. For $^2A_1$ and $^2B_2$ resonances, the scattering electron temporarily occupies the $7a_1$ and $5b_2$ virtual orbital, respectively, and the ion is dissociated leaving one of the fragments in the anionic state. These resonances decay via DEA. We have also calculated the excitation cross section for incident electron energies up to 15 eV, which may aid future experiments. Comparisons are also made between the electron impact cross section for F_2O and Cl_2O target at the same level of complexity. It is shown that Cl_2O cross sections are higher than the corresponding cross sections for F_2O due to the higher nuclear charge of Cl.

[1] K. L. Baluja, N. J. Mason, L. A. Morgan, and J. Tennyson, J. Phys. B **33**, L677 (2000).
[2] K. L. Baluja, N. J. Mason, L. A. Morgan, and J. Tennyson, J. Phys. B **34**, 2807 (2001).
[3] K. L. Baluja, N. J. Mason, L. A. Morgan, and J. Tennyson, J. Phys. B **34**, 4041 (2001).
[4] A. B. Cornford, D. C. Frost, F. G. Herring, and C. A. McDowell, J. Chem. Phys. **55**, 2820 (1971).
[5] C. R. Brundle, M. R. Robin, N. A. Kuehler, and H. Basch, J. Am. Chem. Soc. **94**, 1451 (1972).
[6] J. A. Ibers and Verner Schomaker, J. Phys. Chem. **57**, 699 (1953).
[7] L. E. Sutton and L. O. Brockway, J. Am. Chem. Soc. **57**, 473 (1935).
[8] H. Boersch, Monatsch. Chem. **65**, 311 (1935).
[9] H. J. Bernstein and J. Powling, J. Chem. Phys. **18**, 685 (1950).
[10] A. R. Hilton, A. W. Jache, J. B. Beal, Jr., W. D. Henderson, and R. J. Robinson, J. Chem. Phys. **34**, 1137 (1961).
[11] L. Pierce, R. Jackson, and N. Di Cianni, J. Chem. Phys. **35**, 2240 (1961).

[12] J. W. Bransford, A. C. Kunkle, and A. W. Jache, J. Inorg. Nucl. Chem. **14**, 159 (1960).
[13] J. M. Pochan, R. G. Stone, and W. H. Flygare, J. Chem. Phys. **51**, 4278 (1969).
[14] S. Rothenberg and H. F. Schaefer III, J. Am. Chem. Soc. **95**, 2095 (1973).
[15] K. E. Valenta, K. Vasudevan, and F. Grein, J. Chem. Phys. **72**, 2148 (1980).
[16] W. Thiel, G. Scuseria, H. F. Schaefer III, and W. D. Allen, J. Chem. Phys. **89**, 4965 (1988).
[17] P. Tomasello, M. Ehara, and H. Nakatsuji, J. Chem. Phys. **116**, 2425 (2002).
[18] P. Tomasello, M. Ehara, and H. Nakatsuji, J. Chem. Phys. **118**, 5811 (2003).
[19] L. A. Morgan, C. J. Gillan, J. Tennyson, and X. Chen, J. Phys. B **30**, 4087 (1997).
[20] L. A. Morgan, J. Tennyson, and C. J. Gillan, Comput. Phys. Commun. **114**, 120 (1998).
[21] S. Kaur and K. L. Baluja, J. Phys. B **38**, 3197 (2005).
[22] M. Gupta and K. L. Baluja, J. Phys. B **38**, 4057 (2005).
[23] M. Gupta and K. L. Baluja, Phys. Rev. A **73**, 042702 (2006).
[24] N. Sanna and F. A. Gianturco, Comput. Phys. Commun. **114**, 142 (1998).
[25] *Atomic and Molecular Processes: An R-matrix Approach*, edited by P. G. Burke and K. A. Berrington (Institute of Physics Publishing, Bristol, 1993).
[26] C. J. Gillan, J. Tennyson, and P. G. Burke, *Computational Methods for Electron-Molecule Collisions*, edited by W. M. Huo and F. A. Gianturco (Plenum Press, New York, 1995).
[27] J. Tennyson, J. Phys. B **29**, 6185 (1996).
[28] A. Faure, J. D. Gorfinkiel, L. A. Morgan, and J. Tennyson, Comput. Phys. Commun. **144**, 224 (2002).
[29] K. L. Baluja, P. G. Burke, and L. A Morgan, Comput. Phys. Commun. **27**, 299 (1982).
[30] T. H. Dunning and P. J. Hay, *Methods of Electronic Structure Theory*, edited by H. F. Schaefer (Plenum, New York, 1977), Vol. 2.
[31] E. S. Chang and A. Temkin, Phys. Rev. Lett. **23**, 399 (1969).
[32] F. A. Gianturco and A. Jain, Phys. Rep. **143**, 347 (1986).
[33] A. Jain and D. G. Thompson, Comput. Phys. Commun. **32**, 367 (1984).
[34] J. Tennyson and C. J. Noble, Comput. Phys. Commun. **33**, 421 (1984).
[35] S. I. Chu and A. Dalgarno, Phys. Rev. A **10**, 788 (1974).